SFO Science of Fisheries & Oceanography
ISSN 2734-1011 (Print)
ISSN 2671-4310 (Online)
Vol. 32, No. 2, pp. 81-91 (2023)
https://doi.org/10.22714/SFO.2023.32.2.2

Original Research Article

Numerical Model Analysis of an Abalone Aquaculture Farm Structure for Deployment in the Open Ocean Environment

Taeho Kim[1,*]

[1]Department of Marine Production Management, Chonnam National University, Yeosu 59626, Republic of Korea

* Correspondence to Taeho Kim
E-mail: kimth@jnu.ac.kr

Received September 5, 2023
Revised December 19, 2023
Accepted January 5, 2024

Abstract : In this study, a floating abalone farm system is analyzed using numerical modeling techniques. The floating structure is 24.5 m long and 12.5 m wide with 32 individual containment units deployed in a 4×8 configuration. The primary structural members are pipe made of high-density polyethylene with pinned connections forming walkways. The walkways are kept above the surface with Styrofoam billets. Nets are hung in each of the 32 squares that contain shelters for housing the abalone. A combination fluid-structure hydrodynamic and structural model of the farm was built to analyzed system response to environmental forcing. The model was loaded using combinations of forcing load cases induced by irregular waves and current velocities. Six load cases were simulated in two orthogonal directions. The conditions consisted of (1) a steady current of 1.0 m/s with an exponential decay to the bottom, (2) a JONSWAP irregular wave spectrum (H_{mo} = 5.7 m, T_p = 10.93 s), and (3) the irregular wave superimposed with the 1.0 m/s current decreasing with depth according to a power-law variation. With these conditions and orientations, hydrodynamic loads and critical stresses were calculated.

Keywords : Abalone aquaculture, Finite element modeling, Floating body response, Mooring system tensions, Structural analysis

Introduction

With the rising demand for sustainable seafood sources, aquaculture structures designed for energetic marine environments are becoming increasingly important. Unlike the offshore oil and gas industry, the seafood industry does not have the same level of capital resources to invest in engineering design. In response to these limitations, the efficient use of computer modeling techniques coupled with practical experience would greatly contribute to the design of suitable structures to substantially increase aquaculture production. However, the strengths and limitations of computer models must be understood, as adopting a black-box approach could render analysis results that might lead to structural failure.

Aquaculture systems have recently been developed for raising Pacific abalone (*Haliotis discus hannai*). This species is a valuable product that is commercially available in the Republic of Korea. Commercial-scale abalone production in Korea began in 2000 after several years of research and development, and the country is currently the second-largest producer of cultured abalone in the world, with 23,061 tons produced in 2021 (KOSIS, 2022). Abalones are also cultured in southern Korea, particularly in the coastal waters of the Jeonnam provinces, where *Haliotis discus hannai* is the most common species. These sites, however, often undergo high energy conditions such as strong oceanic currents and irregular waves, especially during typhoon events (Kim and Oh, 2016). Therefore, the use of numerical models to produce accurate results with a high degree of confidence is necessary to reduce the risk of system failures.

In the past 20 years, many numerical approaches have been developed to simulate the dynamics associated with marine aquaculture installations. For example, Gignoux and Messier (1999) applied a commercially available finite element (FE) program to study fish cage dynamics in simulated waves. Lader and Fredheim (2006) introduced a "super element" to represent both hydrodynamic and structural forces on a net panel. In a series of publications, Huang *et al.* (2006, 2016, 2018) performed both numerical and modeling tests to analyze net cage structures. Furthermore, Zhao and collaborators conducted extensive studies of drag and inertia forces on net panels and fish cages through numerical simulations and experimental studies [e.g., Zhao *et al.* (2007, 2008), Dong *et al.* (2010), Bi *et al.* (2014, 2018)]. Berstad and Tronstad (2005) discussed the use of custom-designed simulation software for the hydrodynamic analysis of fish farms. Nicoll *et al.* (2011) used a custom-developed FE solver for the analysis of flexible systems with multi-body interaction in the marine environment, as well as to study the dynamic response of finfish farms under various loading scenarios. Studies have also focused on engineering analyses of the hydrodynamic forces and structural strength of abalone cage system (Kim *et al.*, 2014, 2018).

Moreover, Berstad and Heimstad (2019) and Tsarau and Kristiansen (2019) have recently reported breakthroughs in the development of the FE software packages AquaSim and FhSim, respectively, for modeling fish farm systems.

The development of abalone aquaculture technology for the open ocean requires a rigorous engineering approach if structures are to maintain integrity when subjected to strong storms. The engineering approach should include a combination of physical model tests, field experience and numerical model simulations. Physical models have been used extensively for comparison purposes as described, for example, in Fredriksson *et al.* (2003) and DeCew *et al.* (2005). Field and operational experience is also an important component of the design process to make sure that solutions make sense and therefore practical.

Numerical models are perhaps the most versatile of the engineering design tools since a wide range of concepts and environmental conditions can be considered in a timely fashion. The objective of this study is to perform a set of numerical model simulations of a traditional, floating abalone farm to determine hydrodynamic loads and critical stresses of the floating abalone farm structure.

Materials and Methods

1. Abalone containment structure

The application of the model involved the representation of a traditional abalone cage design employed in the waters of Wando in Korea as shown in Fig. 1a and 1b. In general, the abalone containment structure is 24.5 m long and 12.5 m wide and consists of long members of high-density polyethylene (HDPE) pipe with an outer diameter of 0.11 m. The HDPE pipes are configured as square walkways with a width of 0.5 m. The particular system analyzed was deployed in a depth of about 15 m with a bottom sediment

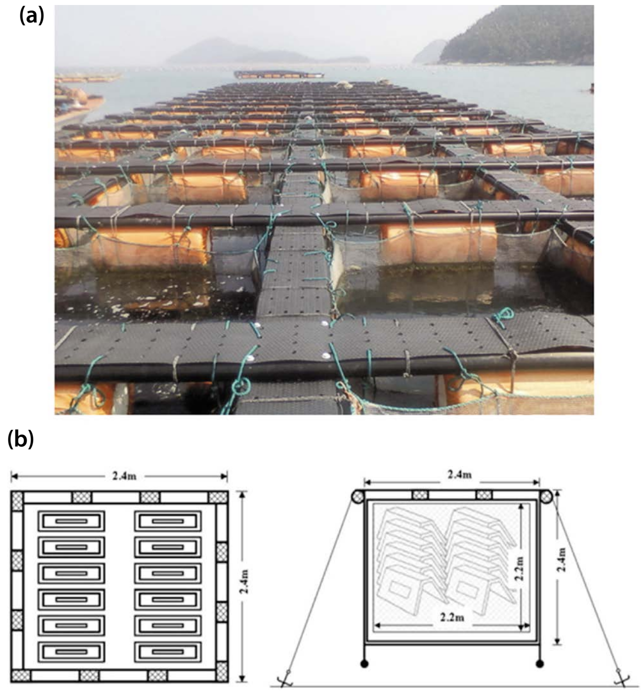

Fig. 1. (a) A traditional abalone containment structure deployed in the waters of Wando, (b) Abalone shelters are placed inside each of the 2.4 m squares.

type of sandy-mud. The cross members of pipe are pinned with galvanized steel bolts at each of the corners in four locations. Buoyancy is provided with 2×0.5 m Styrofoam floats strapped to the HDPE pipe with rope. Within each of the squares, polyethylene nets (Td 380×60 ply) with a half-mesh size ($w_{1/2}$) of 30.3 mm and a twine diameter (td) of 2.6 mm, are suspended from the walkways. Twelve stacks of abalone shelters are placed within each of the squares (Fig. 1b). Mooring lines are attached to the HDPE pipe. The relatively simple system has been known to fail when exposed to typhoon like storms in the region.

2. Loading conditions

The environmental conditions for which the structure analysis was conducted included combinations of waves and currents. The spectrum applied in the model was a form of the Joint North Sea Wave Project (JONSWAP) spectrum (Hasselman *et al.*, 1973) described in Isherwood (1987) as

$$S_\eta(f) = \alpha g^2 (2\pi)^{-4} f^{-5} \exp\left[-1.25\left(\frac{f}{f_m}\right)^{-4}\right]\gamma^b \qquad (1)$$

$$\text{where} = \exp\left[-\frac{(f-f_m)^2}{2\sigma^2 f_{m]}^2}\right],$$

$$\sigma = \sigma_a \quad \text{for } f \le f_m \text{ and } \sigma = \sigma_b \text{ for } f > f_m.$$

In equation (1), f is the frequency in Hz, f_m is the peak frequency associated with the maximum value of $S(f)$ with the terms α, γ and σ as fitting parameters. The peak frequency is also the inverse of the dominant wave period (T_p). According to Isherwood (1987), the relationship between the peak frequency and the average wave period (T_z) is curve fit calculated according to

$$T_z = \frac{\left(0.6063 + 0.1164\gamma^{1/2} - 0.01224\gamma\right)}{f_m}, \tag{2}$$

valid for $0.6 < \gamma < 8.0$. With the average wave period, a wave steepness term(s),

$$s = \frac{2\pi H_s}{g T_z} \tag{3}$$

is found to calculate the curve fitting parameter,

$$\alpha = s^2\left(2.964 + 0.4788\gamma^{1/2} - 0.3430\gamma + 0.04225\gamma^{3/2}\right). \tag{4}$$

The wave spectral shape was then determined with $\sigma_a = 0.07$, $\sigma_b = 0.09$ and $\gamma = 1$. For the simulations presented here, a significant wave height (H_s) and dominant period (T_p) of 5.7 m and 10.93 s were used respectively. These values were chosen according to the design wave conditions for the vicinity of Wando, Korea over a 10-year return period (http://www.kiost.ac). The corresponding spectral shape is shown in Fig. 2.

In addition to the irregular waves, a constant current velocity (V) of 1.0 m/s was also applied in the same direction according to

$$V(z) = V_b + \left(V_f + V_b\right)\left[\frac{z - z_b}{z_f - z_b}\right]^{1/exponent}, \tag{5}$$

where V_f and V_b are the velocity magnitude values at the vertical locations of $z_f = 0$ (surface) and $z_b = 15$ m, respectively. In this application, an exponent value equal to 3 was applied. Load cases for the model included the two abalone farm orientations as shown in Fig. 3. Load case #1 in Fig. 3 has a wave and current orientation normal to the smaller dimension of the farm, while load case #2 has a wave and current orientation normal to the larger dimension of the farm. Simulations were performed with the numerical model to assess the hydrodynamic loads on the system, mooring line tensions and structural stresses in the floating abalone farm structure. Load cases included combinations of JONSWAP irregular waves and steady currents and consisted of (1) currents applied according to equation (5), (2) irregular waves described

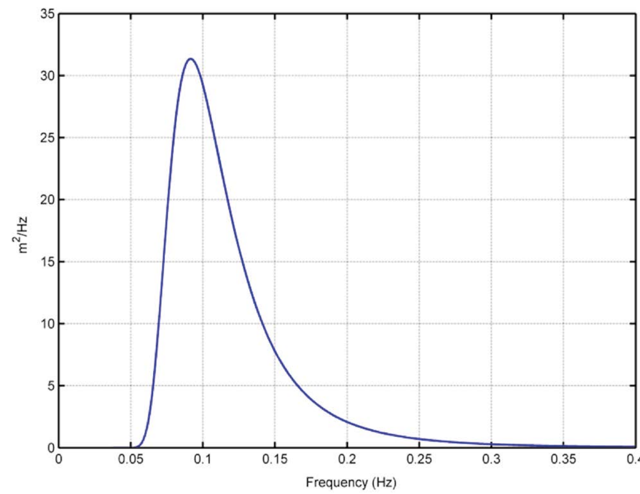

Fig. 2. Numerical model input wave spectrum with an $H_{m0} = 5.7$ m and a $T_p = 10.93$ s.

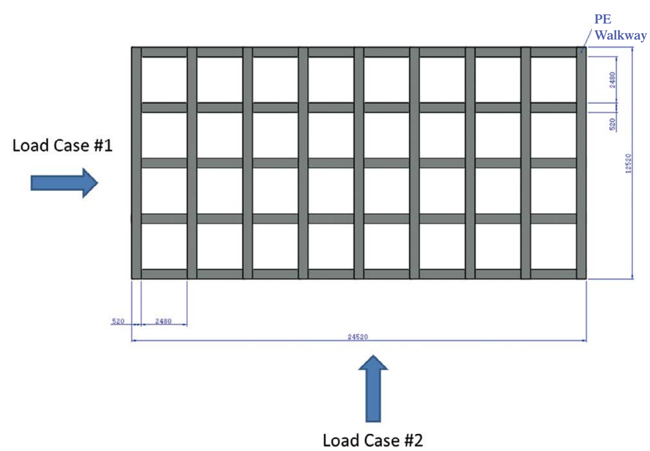

Fig. 3. Load case directions used in the numerical modeling study.

by equations (1)~(4), and (3) a superimposed combination of load cases (1) and (2).

3. Numerical model and structure

1) Numerical model

The model performs hydrodynamic simulations using a commercial general-purpose, finite element (FE) solver. The environmental forces (buoyancy, drag and inertia) are calculated using a user-defined force subroutine based on a modified Morison equation (Morison *et al.*, 1950),

$$\frac{\partial \vec{F}}{\partial l} = \frac{1}{2}\rho_w D C_n \left| U_{Rn} \right| \vec{U}_{Rn} + C_t \vec{U}_{Rt} + \rho_w A \dot{\vec{U}}_n + \rho_w A C_m \dot{\vec{U}}_{Rn}. \tag{6}$$

In equation (6), is the fluid force per unit length, and are the normal and tangential components of the fluid particle velocity relative to the element velocity, is the normal component of absolute fluid particle acceleration, is the normal component of the fluid particle acceleration relative to the element acceleration. Also in equation (6), kg m^{-3} is the water density, is the diameter of the cylinder, is the external cross-sectional area (i.e. the same water-tight cross-sectional area as used for buoyancy calculations), is the normal drag coefficient, is the tangential drag coefficient and is the added mass coefficient. Fluid particle velocity and acceleration fields are calculated using the linear wave theory described in Dean and Dalrymple (1991). For the case of irregular seas, the profile can be approximated using the linear superposition of waves,

$$\eta(x,t)=\sum_{i=1}^{N}\frac{H_i}{2}\ \cos\left[\left(k_i x-(2\pi f_i)t+\theta_i\right]\right. \tag{7}$$

where H_i are the wave heights, k_i are the wave numbers, x is the horizontal position with respect to the origin, f_i are the wave frequencies and θ_i are the random phase components. Even though the present approach does not account for surface effects for the bodies floating at the waterline, effect of partial submergence is considered by evaluating the submerged volume fraction. This parameter is used as a multiplier for buoyancy, drag and inertial forces, thus gradually accounting to transition from the dry to submerged states.

2) Geometric and material properties

An important component of the procedure was the appropriate use geometric and material properties as provided in Table 1. With the geometric and material properties, the numerical model of the abalone farm system was constructed with truss and beam elements. As shown in Fig. 4a, beam elements were used for the Styrofoam flotation, HDPE pipe and the galvanized steel bolts. Flexible connectors such as the rope, nets and mooring components were modeled as trusses. The walkways shown in Fig. 4a lashed to the HDPE were not modeled because it was assumed that these plastic sheets do not affect structural response of the system. It should be noted that even though presence of abalone shelters within the containment nets would significantly increase the drag on the system, these components were excluded from the analysis in this study. Anchoring locations on the seafloor bottom were modeled as fixed points.

In the model, the abalone cage system was secured by 8 mooring legs in the positions shown in Fig. 4b. In 15 m of water and at an approximate scope of 3 : 1, each leg consisted of 45 m of 48 mm rope. At the corners, anchor legs extended out 45 degrees. Anchor points were modeled as fixed points with no chain catenaries.

Table 1. Geometric and material properties used in each modeling approach

Component	Element	Parameter	Value
Pipe	02-pipes	Diameter DR rating Material Mass density	114 mm 17 HDPE 950 kg/m^3
Floats	03-floats	Length Diameter Material Mass density	2 m 0.5 m Styrofoam 300 kg/m^3
Bolts	04-bolts	Length Diameter Material Mass density	0.125 m 50 mm Steel 7870 kg/m^3
Float rope	05-float rope	Length Diameter Material Mass density	0.707 m 42 mm Polypropylene 1100 kg/m^3
Net	06-net-side 07-net-bottom	Twine diameter Half-mesh Ply Material Mass density	2.6 mm 30.3 mm 60 Polyethylene 1485 kg/m^3
Net connectors	08-net-connectors	Length Diameter Material Mass density	2.46 m 12 mm Polypropylene 1100 kg/m^3
Net weights	09-net-weights Not analyzed	Material Mass in air Number per chamber Shape Mass density	Concrete 15 kg 4 Cylinder 2400 kg/m^3
Mooring lines	10-mooring-lines	Diameter Length Material Mass density	48 mm 45 Polypropylene 1100 kg/m^3

The net of an aquaculture structure is one of the most dominant features of the entire system. It is typically compliant undergoing large displacements in storm conditions and induces a substantial component of total loading due to fluid-structure interactions. Building a numerical representation of the net, however, is not trivial requiring accurate geometric and material properties (Moe *et al.*, 2007) and specific

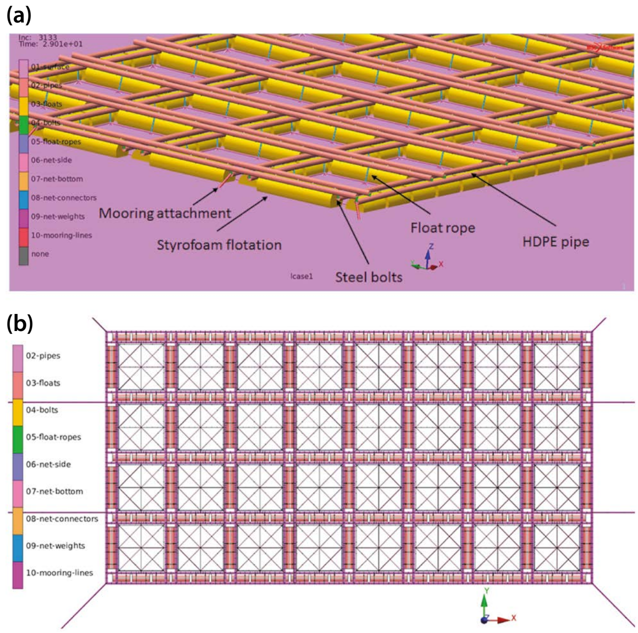

Fig. 4. (a) The numerical model construction of the traditional abalone farm structure, (b) The eight mooring leg locations and a plan view of the numerical model of the traditional abalone grow out system.

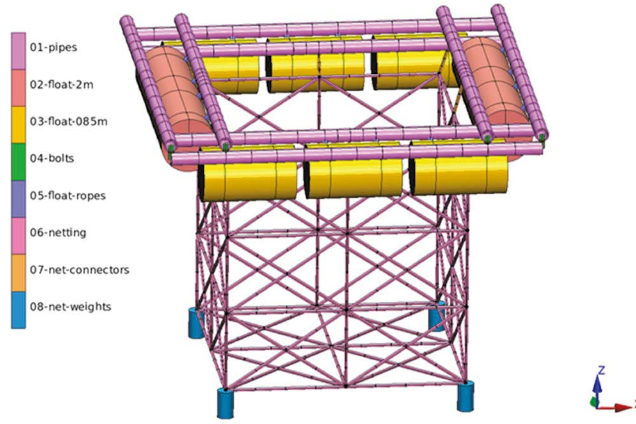

Fig. 5. Suspended net construction in the numerical model.

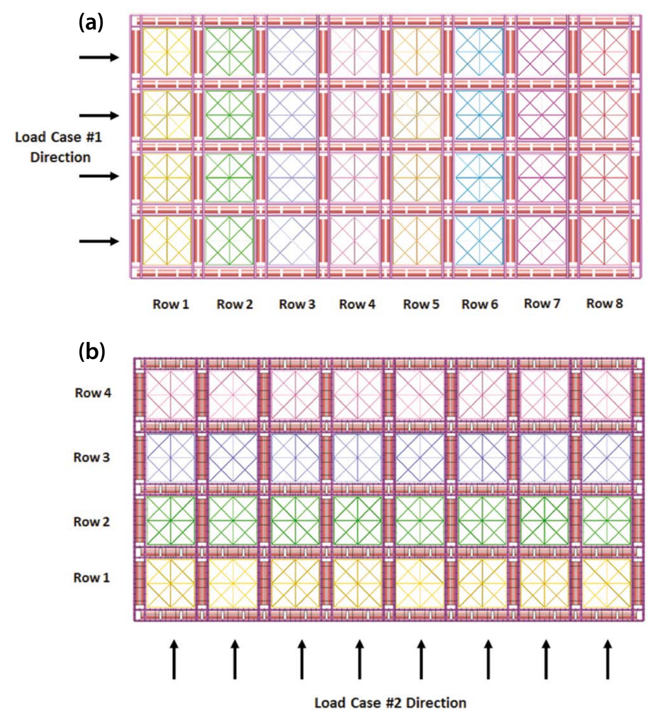

Fig. 6. (a) Net shadowing configuration for load case #1, (b) Net shadowing configuration of load case #2.

modeling approaches (Tsukrov *et al.*, 2003; Fredriksson *et al.*, 2014).

It is also computationally expensive to account for every twine of the construction (a typical net can be comprised of approximately 100 twines with about 2500 intersections per m^2). The net needs to be simplified in such a way that the fluid loads are redistributed on a simplified mesh and the representative behaviors of the net panels are not compromised. The net modeling technique considered for both the model is based on the "consistent net element" approach of Tsukrov *et al.* (2003). By knowing the half-mesh width ($w_{1/2}=30.3$ mm) and the twine diameter ($td=2.6$ mm), the solidity (S) of the net was calculated according to

$$S=\frac{2t_d}{w_{1/2}}-\left(\frac{t_d}{w_{1/2}}\right)^2. \tag{8}$$

With the outline area, solidity and twine diameter, the total length of the twine in the panel was then estimated. A new parameter called net length-ratio is defined as total twine length divided by the total net element length created in the model. An equivalent twine cross-sectional area was determined by setting the material volume of the model net equal to that of the actual net multiplied by the length-ratio (i.e. consistent mass/volume representation). Having equal volumes, bulk net panel properties including weight, buoyancy, and inertia with added mass are matched in each model. With the same volume, however, the projected area of the panel was less than that of the actual net. To match drag forces, the equivalent diameter is calculated as actual twine diameter multiplied by the net length-ratio.

Prescribing an appropriate drag coefficient for netting was also necessary and has been the topic of numerous studies. A review of much of this work can be found in Tsukrov *et al.* (2011). For example, previous approaches have utilized drag coefficients that are updated at every time step based on Reynolds number (Choc and Casarella, 1971; DeCew *et al.*,

2010) or empirical forms described in Milne (1972), Aarnse *et al.* (1990), Zhan *et al.* (2006) and Balash *et al.* (2009). The approach taken in this study is from Tsukrov *et al.* (2011) with a nominal value of 1.4 considering nearly all of the sources presented. It was also discussed in this paper that drag coefficient values did not exhibit a strong dependence on Reynolds number or solidity. In addition to the drag coefficient, the added mass coefficient is also used in the inertia terms of the Morison equation shown by equation (6). For this application, a standard value of 1 was utilized consistent for submerged circular cylinders.

An important aspect of the modeling configuration is the reduction of mean horizontal velocities due to turbulence induced by the nets often referred to net shadowing. In general, the magnitude of the velocity is reduced as a function of net solidity. Flow reduction within the model, however, was represented as a function of cage row for each orientation as shown on Fig. 6a and 6b. In the calculations, a reduction value of 15% was applied through each cage row according to the work described in Aarnses *et al.* (1990).

4. Structural analysis of integrity of pipes

Since the anchors were modeled as fixed points, the corresponding structural response of the individual components of the farm could then be analyzed as if the anchors held. As a reporting result, an extensive amount of data was produced from the six simulations. For seven of the eight element types provided in Table 1, engineering parameters were calculated. The engineering parameter for the truss elements was axial force (kN).

Since the model shown in Figs. 4~6 has nearly 43,000 elements, to perform the data processing procedure and examine the results, code was written to organize the calculated data sets into the seven element types. If the element was configured as a beam, the data set was further organized into the six engineering parameters listed above. If the element was configured as a truss, then only the tension was stored (i.e. positive axial force). The information in each of these files was then sorted from the largest positive number to the corresponding negative number (direction related).

1) Maximum equivalent stress calculations

The integrity of the HDPE pipe supporting the structure was analyzed by processing the result files of the model simulations. Using a Python script, values of axial force (F), bending moment (M_x) bending moment (M_y) and torque (T) were collected from the model simulations for all beam elements comprising the HDPE pipes. The value of equivalent (von Mises) stress was then calculated for every integration point of HDPE pipe beam elements.

The general expression of the equivalent stress in the Cartesian coordinate system is

$$\sigma_{eq}=\sqrt{\frac{1}{2}\left[(\sigma_{xx}-\sigma_{yy})^2+(\sigma_{yy}-\sigma_{zz})^2+(\sigma_{zz}-\sigma_{xx})^2+6(\sigma_{xy}^2+\sigma_{yz}^2+\sigma_{zx}^2)\right]}. \tag{9}$$

In the cylindrical coordinate system the expression becomes,

$$\sigma_{eq}=\sqrt{\frac{1}{2}\left[(\sigma_{rr}-\sigma_{\theta\theta})^2+(\sigma_{\theta\theta}-\sigma_{zz})^2+(\sigma_{zz}-\sigma_{rr})^2+6(\sigma_{r\theta}^2+\sigma_{\theta z}^2+\sigma_{zr}^2)\right]}. \tag{10}$$

where A is the area of the pipe's cross-section, r_0 is the outer radius of the pipe, I_{xx} is the second moment of the cross-sectional area of the pipe around x-axis, and J_{xy} is the polar moment of the cross-sectional area around the center. For the given pipe with $r_0=0.0625$ m, internal radius $r_i=0.0510$ m and wall thickness $t=0.0115$ m.

In thin-walled pipes, in the absence of the internal pressure the components σ_{rr} and $\sigma_{\theta\theta}$ are zero. The shear components $\sigma_{\theta z}$ and σ_{zr} can be neglected since they are zero near the surface part of the pipe under theses loading conditions. The final expression for the equivalent stress reduces to

$$\sigma_{eq}=\sqrt{\sigma_{zz}^2+3\sigma_{r\theta}^2}, \tag{11}$$

where $\sigma_{zz}=\sigma^F_{zz}+\sigma^M_{zz}$ is the combination of normal stresses due to axial force and bending moments, and $\sigma_{r\theta}$ is the shear force due to applied torque. The normal stresses σ^F_{zz} and σ^M_{zz}, and shear stress $\sigma_{r\theta}$ are found as

$$\sigma^F_{zz}=F/A, \tag{12}$$

$$\sigma^M_{zz}=\frac{r_o\sqrt{M_x^2+M_y^2}}{I_{xx}}, \tag{13}$$

$$\sigma_{r\theta}=\frac{r_oT}{J_{xy}}, \tag{14}$$

where A is the area of the pipe's cross-section, r_0 is the outer radius of the pipe, I_{xx} is the second moment of the cross-sectional area of the pipe around x-axis, and J_{xy} is the polar moment of the cross-sectional area around the center. For the given pipe with $r_0=0.0625$ m, internal radius $r_i=0.0510$ m and wall thickness $t=0.0115$ m,

$$A=41.01\cdot10^{-4}\,\mathrm{m}^2,\ I_{xx}=6.67\cdot10^{-6}\,\mathrm{m}^4,\ J_{xy}=13.34\cdot10^{-6}\,\mathrm{m}^4.$$

2) Stress calculations using finite element analysis

In addition to the analytical predictions of the maximum equivalent stress, finite element analysis of a pipe was per-

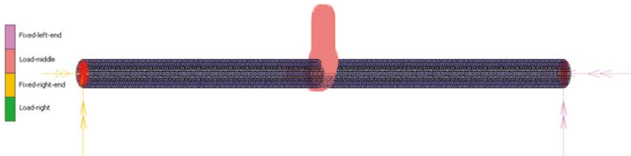

Fig. 7. The boundary conditions for the HDPE pipe model.

formed subjected to forces and moments that corresponding to the highest value of σ_{eq}. After performing mesh sensitivity studies, the FE model was generated using 7,488 quadratic 20-node hexagonal elements. The model diagram illustrating boundary conditions used in the model is shown in Fig. 7.

Results and Discussion

1. Motions and anchor leg tensions

The results of the six model simulations were analyzed for mooring leg tensions, vertical displacements of the forward and aft points on the surface structure and local engineering parameters for the structural components. The points and mooring locations are shown in Fig. 8a and 8b for load case #1 and #2, respectively.

The vertical displacement results for the forward and aft points were investigated for the waves only case for each load case direction. The time series results for the forward and aft points are shown in Fig. 9 for load case #1 and #2. The basic statistics including the maximum, minimum and standard deviation for each of the time series are provided in Table 2. The significant response values defined as four times the square root of the variance divided by significant wave height of the spectrum is also provided in Table 2.

The tensions in the corner and main moorings were also examined, but for the wave and currents load case directions. The orientations of the mooring lines are shown in Fig. 8a and 8b. Main and corner tension value time series are shown in Fig. 10. For load case #1, both main corner tensions are provided, while only the corner mooring leg values are shown for load case #1. The basic statistics associated with the data sets are provided in Table 3.

While the intent of this study was to present analysis results, it is interesting to note that based on the failure of the system shown in the picture in Fig. 11, it is possible that anchor moorings were the weakest part of the system. The picture shows the farm wash-up on the shore, mostly intact, though heavily deformed. Since the numerical approach modeled the anchors as fixed points, with the anchor line

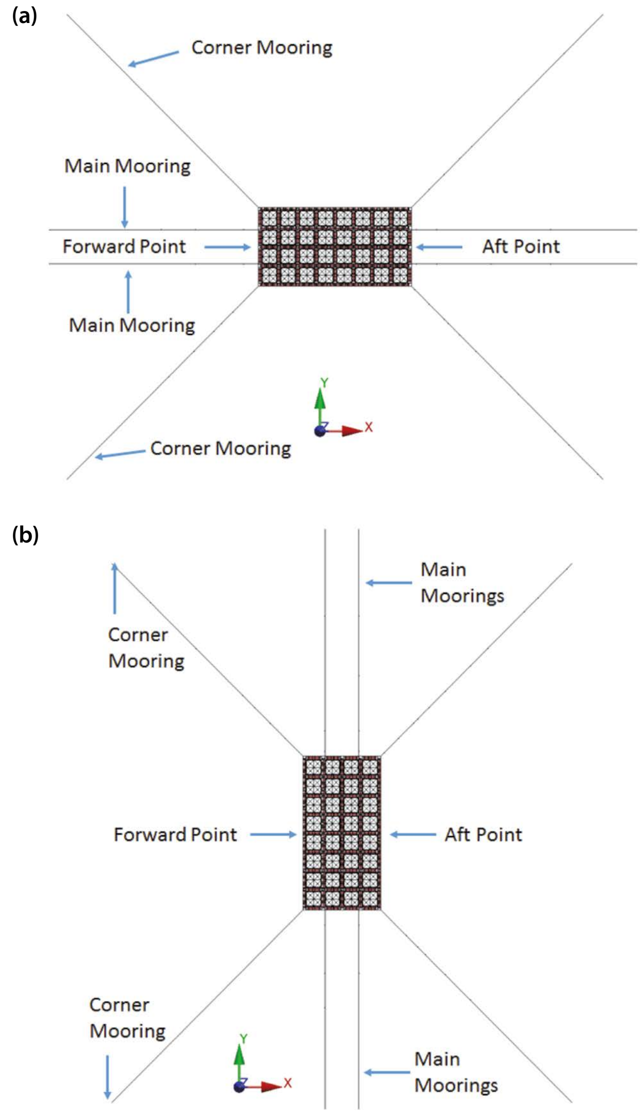

Fig. 8. Model results were investigated for surface structure point movements (forward and aft) and corner and mooring line tensions in the load case #1 (a) and #2 (b) configurations.

tensions calculated, it can be determined at what tension the corresponding anchors will pull-out or slide depending upon the specific design used.

2. Structural stress of HDPE pipe

It can be seen that the highest value of $\sigma_{eq}^{(max)} = 181.24$ MPa is found in one of the HDPE pipe beam elements. According to the tabular values, the yield stress of the HDPE, which means the predicted stress values are 7.55 times higher than allowable based on these calculations.

In addition to the calculations of equivalent stresses, individual stress components, σ_{zz}^{F}, σ_{zz}^{M} and $\sigma_{r\theta}$ corresponding

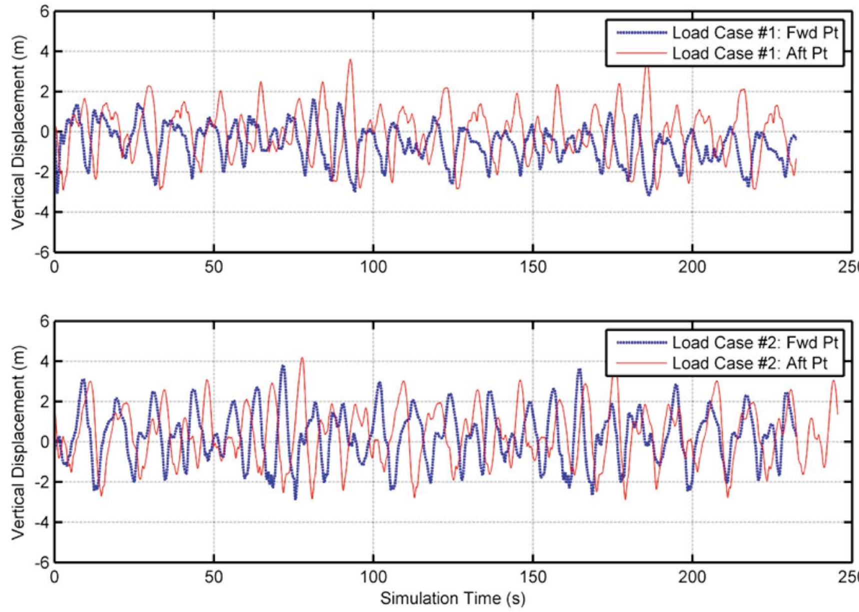

Fig. 9. Vertical time series results for the forward and aft points on the surface structure.

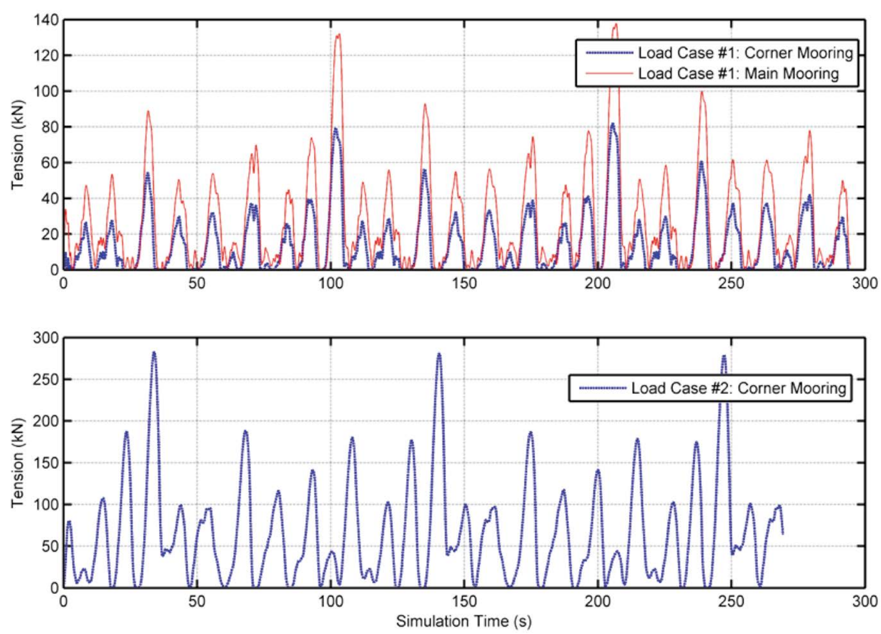

Fig. 10. Corner and main mooring leg time series for each load case directions.

to the maximum values of axial force, equivalent bending moment. In these plots, black curves correspond to the normal stresses due to bending, red are the normal stresses due to axial forces and blue curves are shear stresses due to torque. According to the plots, the most significant contribution to the equivalent stresses comes from bending, which is consistent with the observed large deformations of the raft structure.

The left end of the pipe was fixed (both rotations and displacements), the right end was also fixed except for the rotation around the pipes longitudinal axis. Forces and were applied (distributed over several nodes to avoid stress localization) to produce maximum bending moments and in the middle of the pipe. Longitudinal force and torque were applied

Table 2. Characteristic motion response values for load case #1 and #2

Parameter	Max (m)	Min (m)	Std (m)	Normalized response (m/m)
Load case #1				
Fwd point	1.64	−3.16	0.92	3.68/5.7 = 0.64
Aft point	3.60	−2.92	1.30	5.20/5.7 = 0.91
Load case #2				
Fwd point	3.81	−2.87	1.34	5.34/5.7 = 0.94
Aft point	4.22	−2.87	1.42	5.69/5.7 = 1.00

Table 3. Tension response for load case #1 and #2

Parameter	Max (kN)	Mean (kN)	Std (kN)
Load case #1			
Corner	81.93	13.99	16.51
Main	137.80	26.97	27.42
Load case #2			
Corner	282.71	65.79	60.88
Main	–	–	–

Fig. 11. Abalone farm destruction as a result of a specific storm event (https://m.khan.co.kr/national/incident/article/201208282200045#c2b).

at the right end of the pipe. The resulting von Mises stress distribution is shown in Fig. 12.

According to the plots, the maximum von Mises stress observed is 181 MPa, which is within 1% of the analytically predicted value. This confirms that analytical calculations (which assume small deformations) are sufficient to predict maximum stresses even for a large deformation case under the considered loading conditions.

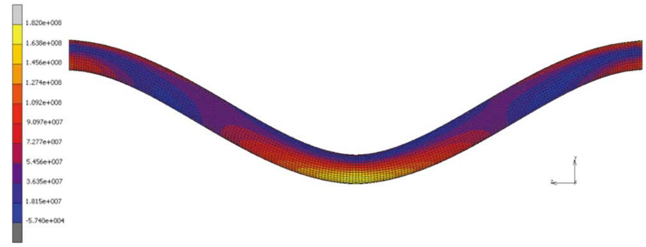

Fig. 12. von Mises stresses calculated with the FE model.

Conclusions

In this study, a numerical model of these abalone structures was built within a FEM and configured with two directional load cases that included irregular waves and currents that decreased exponentially in magnitude with depth. Model forcing was implemented in the code with a form of Morison equation to represent fluid-structure interactions. Mooring line tensions and structure motions were presented as part of this initial modeling procedure. The results showed that maximum mooring tension in load case #1 were on the main moorings (138 kN) and on the corner moorings for load case #2 (283 kN). The structural also showed wave following characteristics for each load case with reduced motion on the leading edge due to the mooring attachments. These results are presented considering that the anchors were modeled as fixed points.

The loads from the fluid-structure interaction modeling were then used in another part of the modeling approach to calculate stresses in the primary components of the structure consisting of HDPE pipe. The results were then post-processed to obtain equivalent (von Mises) stresses. The highest value was found to be 181 MPa, one of the HDPE pipe beam elements. According to the tabular values, the yield stress of the HDPE, which means the predicted stress values are 7.55 times higher than allowable based on these calculations. Once again, these values were calculated based on the initial condition of fixed anchor points.

Qualitative information suggests that the anchors did indeed move so that the tensions in the mooring and stresses in the pipe may not have actually reached the levels presented in this study based on the fixed mooring configuration. The next step would be to fully analyze the individual mooring leg design configurations to perhaps included compliance with chain, compensator buoys, elastic line or other acceptable technique.

References

Aarsnes, J., H. Rudi and G. Loland, 1990. Current forces on cage, net deflection. In Engineering for Offshore Fish Farming. Thomas Telford, pp. 137-152.

Balash, C., B. Colbourne, N. Bose and W. Raman-Nair, 2009. Aquaculture net drag force and added mass. *Aquacultural Engineering,* 41(1), 14-21.

Berstad, A.J. and H. Tronstad, 2005. Response from current and regular/irregular waves on a typical polyethylene fish farm Maritime Transportation and Exploitation of Ocean and Coastal Resources. Eds. C. Guedes Soares, Y. Garbatov, N. Fonseca. 2005 Taylor & Francis Group London.

Berstad, A.J. and L.F. Heimstad, 2019. Analysis of flexible net structures in marine environment. Proceedings of VIII International Conference on Computational Methods in Marine Engineering MARINE 2019, R. Bensow and J. Ringsberg (Eds).

Bi, C.W., Y.P. Zhao, G.H. Dong, Y.N. Zheng and F.K. Gui, 2014. A numerical analysis on the hydrodynamic characteristics of net cages using coupled fluid-structure interaction model. *Aquacultural Engineering*, 59, 1-12.

Bi, C.W., Y.P. Zhao, G.H. Dong, Z.-M. Wu, Y. Zhang and T.-J. Xu, 2018. Drag on and flow through the hydroid-fouled nets in currents. *Ocean Engineering*, 161, 195-204.

Choc, Y.I. and M.J. Casarella, 1971. Hydrodynamic resistance of towed cables. *Journal of Hydronautics*, 5(4), 126-131.

Dean, R.G. and R.A. Dalrymple, 1991. Water Wave Mechanics for Engineers and Scientists, 2nd ed., Singapore: World Scientific Publishing Company, Singapore, 66-69.

DeCew, J., D.W. Fredriksson, L. Bougrov, M.R. Swift, O. Eroshkin and B. Celikkol, 2005. Numerical and physical modeling of a modified gravity type cage and mooring system. *IEEE Journal of Oceanic Engineering*, 30(1), 47-58.

DeCew, J., I. Tsukrov, A. Risso, M.R. Swift and B. Celikkol, 2010. Modeling of Dynamic behavior of a single-point moored submersible fish cage under currents. *Aquacultural Engineering* 43, 38-45.

Dong, G.W., S.H. Hao, Y.P. Zhao, Z. Zong and F.K. Gui, 2010. Numerical analysis of the flotation ring of a gravity-type fish cage. *ASME Journal of Offshore Mechanics and Arctic Engineering*, 132(3), 031304.

Fredriksson, D.W., J. DeCew, P. Lader, Z. Volent, O. Jensen and F.V. Willumsen, 2014. A finite element modeling technique for an aquaculture nets with laboratory measurement comparisons. *Ocean Engineering*, 83, 99-110.

Fredriksson, D.W., M.R. Swift, J.D. Irish, I. Tsukrov and B. Celikkol, 2003. Fish cage and mooring system dynamics using physical and numerical models with field measurements. *Aquacultural Engineering*, 27(2), 117-146.

Gignoux, H. and R.H. Messier, 1999. Computational modeling for finfish aquaculture net pens. *Oceanic Engineering International. St. John's, NF*, 3(1), 12-22.

Hasselmann, K., T.P. Barnett, E. Bouws, H. Carlson, D.E. Cartwright, K. Enke, J.A. Ewing, A. Gienapp, D.E. Hasselmann, P. Kruseman and A. Meerburg, 1973. Measurements of wind-wave growth and swell decay during the North Sea Wave Project (JONSWAP). Ergaenzungsheft zur Deutschen Hydrographischen Zeitschrift,, Reihe A.

Huang, C.C., H.H. Tang and J.Y. Liu, 2006. Dynamic analysis of net cage structures for marine aquaculture: Numerical simulation and model testing. *Aquacultural Engineering*, 35(3), 258-270.

Huang, X.H., G.X. Guo, Q.Y. Tao, Y. Hu, H.Y. Liu, S.M. Wang and S.H. Hao, 2016. Numerical simulation of deformations and forces of a floating fish cage collar in waves. *Aquacultural Engineering*, 74, 111-119.

Huang, X.H., G.X. Guo, Q.Y. Tao, Y. Hu, H.Y. Liu, S.M. Wang and S.H. Hao, 2018. Dynamic deformation of the floating collar of a net cage under the combined effect of waves and current. *Aquacultural Engineering*, 83, 47-56.

Isherwood, R.M., 1987. A revised parameterisation of the JONSWAP spectrum. *Applied Ocean Research*, 9(1), 47-50.

Kim, T. and M.-H. Oh, 2016. Submersible cage system for abalone aquaculture - Design for open sea can avoid extreme wind, waves. *Sea Technology*, 57(6), 33-35.

Kim, T., J. Lee, D.W. Fredriksson, J. DeCew, A. Drach and K. Moon, 2014. Engineering analysis of a submersible awbalone aquaculture cage system for deployment in exposed marine environments. *Aquacultural Engineering*, 63, 72-88.

Kim, T., J. Lee, D.W. Fredriksson, J. DeCew, A. Drach and S.C. Yim, 2018. Design approach of an aquaculture cage system for deployment in the constructed channel flow environments of a power plant. *PLos One*, 13(6), e0198826.

KOSIS, 2022. Total Fishery Production. Received from https://kostat.go.kr.

Lader, P.F. and A. Fredheim, 2006. Dynamic properties of a flexible net sheet in waves and current - A numerical approach. *Aquacultural Engineering*, 35(3), 228-238.

Milne, P.H., 1972. Fish and shellfish farming in coastal waters. Fish News (Books), London, U.K.

Moe, H., A. Olsen, O.S. Hopperstad, O. Jensen and A. Fredheim, 2007. Tensile properties for netting materials used in aquaculture net cages. *Aquacultural Engineering*, 37(3), 252-265.

Morison, J.R., J.W. Johnson, M.P. O'Brien and S.A. Schaaf, 1950. The forces exerted by surface waves on piles. *Journal of Petroleum Technology*, 2(5), 149-154.

Nicoll, R.S., D.M. Steinke, J. Attia, A. Roy and B.J. Buckham, 2011. Simulation of a high-energy finfish aquaculture site using a finite element net model, Proceedings of the 30th International Conference on Offshore Mechanics and Arctic Engineering, Rotterdam, The Netherlands.

Tsarau, A. and D. Kristiansen, 2019. Application of fhsim for the analysis of environmental loads on a complete fish-farm system. Proceedings of VIII International Conference on Computational Methods in Marine Engineering MARINE 2019, R. Bensow and J. Ringsberg (Eds).

Tsukrov, I., A. Drach, J. DeCew, M.R. Swift and B. Celikkol, 2011. Characterization of geometry and normal drag coefficients of copper nets. *Ocean Engineering*, 38, 1979-1988.

Tsukrov, I., O. Eroshkin, D.W. Fredriksson, M.R. Swift and B. Celikkol, 2003. Finite element modeling of net panels using consistent net element. *Ocean Engineering*, 30, 251-270.

Zhan, J.M., X.P. Jia, Y.S. Li, M.G. Sun, G.X. Guo and Y.Z. Hu, 2006. Analytical and experimental investigation of drag on nets of fish cages. *Aquacultural Engineering*, 35(1), 91-101.

Zhao, Y.P., Y.C. Li, G.H. Dong, F.K. Gui and B. Teng, 2007. A numerical study on dynamic properties of the gravity cage in combined wave-current flow. *Ocean Engineering*, 34, 2350-2363.

Zhao, Y.-P., Y.-C. Li, G.-H. Dong, F.-K. Gui and H. Wu, 2008. An experimental and numerical study of hydrodynamic characteristics of submerged flexible plane nets in waves. *Aquacultural Engineering*, 38, 16-25.